Textural Feature Based Target Detection in Through-the-Wall Radar Imagery

A. Sengur[†a], M. Amin*[b], F. Ahmad[b], P. Sévigny[c], D. DiFilippo[c]
[a] Dept. of Electrical and Electronics Engineering, Faculty of Technology, Firat University, 23119 Elazig, Turkey;
[b]Radar Imaging Lab, Center for Advanced Communications, Villanova University, 800 Lancaster Ave, Villanova, PA 19085, USA;
[c]Radar Sensing and Exploitation, Defence R&D Canada, 3701 Carling Ave., Ottawa, ON, Canada K1A 0Z4.

ABSTRACT

Stationary target detection in through-the-wall radar imaging (TWRI) using image segmentation techniques has recently been considered in the literature. Specifically, histogram thresholding methods have been used to aid in removing the clutter, resulting in 'clean' radar images with target regions only. In this paper, we show that histogram thresholding schemes are effective only against clutter regions, which are distinct from target regions. Target detection using these methods becomes challenging, if not impossible, in the presence of multipath ghosts and clutter that closely mimics the target in size and intensity. Because of the small variations between the target regions and such clutter and multipath ghosts, we propose a textural feature based classifier for through-the-wall target detection. The feature based scheme is applied as a follow-on step after application of histogram thresholding techniques. The training set consists of feature vectors based on gray level co-occurrence matrices corresponding to the target and ghost/clutter image regions. Feature vectors are then used in training a minimum distance classifier based on Mahalanobis distance metric. Performance of the proposed scheme is evaluated using real-data collected with Defence Research and Development Canada's vehicle-borne TWRI system. The results show that the proposed textural feature based method yields much improved results compared to histogram thresholding based segmentation methods for the considered cases.

Keywords: Image segmentation, textural features, target detection, through-the-wall radar, co-occurrence matrix.

1. INTRODUCTION

Through-the-wall radar imaging (TWRI) is emerging as a viable technology for providing vision into optically obscured areas in a variety of important civilian and military applications.[1, 2] Unlike moving targets indoor and behind walls,[3, 4] detection of stationary humans is one of the most challenging and important objectives in TWRI. Biometric features, such as breathing and heartbeat, can be employed for identifying stationary humans. However, the presence of exterior lossy walls prohibits high frequency radar operations in TWRI. As a result, biometric radars can face challenges in detecting micro-Doppler signatures associated with breathing and heart beat behind walls. In this case, detection of stationary humans would solely depend on high fidelity imaging and effective image-domain target detection techniques.

Detection of stationary targets in TWRI using image segmentation techniques has recently been considered in the literature.[5-8] In Refs. [5]-[7], histogram thesholding methods, such as the Otsu's thresholding method[9] and maximum entropy segmentation[10], were used to aid in removing the clutter and detecting target regions. In Ref. [8], a multi-level histogram thresholding approach was presented for automatic target detection. In these publications, the histogram thresholding schemes were shown to be effective in enhancing the images by suppressing clutter regions, which were distinct from target regions. However, in the presence of ghosts resulting from multipath propagation and clutter that closely mimics the target in size and intensity, target detection using these methods becomes challenging.

[†]The work by A. Sengur was performed while he was working as a visiting researcher at the Center for Advanced Communications, Villanova University.

* moeness.amin@villanova.edu; phone 1 610 519-4263; http://www.villanova.edu/engineering/research/centers/cac/

Figure 1. Block Diagram of the Textural Feature based Approach.

In this paper, we investigate the use of texture based features for classifying target and clutter regions in indoor images. More specifically, we propose a textural feature-based target detector, which involves a two-step process. First, a histogram thresholding based image segmentation technique is applied to the input image. The binary image produced by the image segmentation method is masked on the original input image to produce an enhanced image with candidate target regions only. Then, the problem of target recognition from amongst the identified candidates is solved by means of a feature-extraction strategy and a minimum distance classifier based on the Mahalanobis distance metric. Textural features, such as contrast, correlation, energy, and homogeneity, are extracted from gray level co-occurrence matrices (GLCM's). A co-occurrence matrix is the spatial-dependence probability-distribution matrix of pairs of pixels separated by a given offset in a particular direction.[11] Figure 1 shows the block diagram of the proposed feature based target detector.

Both histogram thresholding only and the proposed textural feature based detector are applied to real images acquired with the Multi-channel TWSAR,[12] which is the vehicle-borne through-the-wall radar imaging system developed by Defence Research and Development Canada (DRDC). The dataset corresponds to through-the-wall measurements of multiple humans of different heights, standing or sitting at different locations in an empty room. The performance of the two schemes is assessed in terms of improvement in separation of target from multipath ghosts and clutter in individual images. We show that, for the specific data analyzed, the follow-on textural feature based step provides higher suppression of multipath ghosts and clutter, while successfully maintaining the target regions.

The remainder of the paper is organized as follows. Section 2 reviews the image segmentation methods based on histogram thresholding employed in Refs. [5]-[7]. The gray level co-occurrence based feature extraction and minimum Mahalanobis distance classifier are described in Section 3. Section 4 evaluates the performance of the image segmentation only and feature based methods using real data. Section 5 contains the concluding remarks.

2. IMAGE SEGMENTATION

In this section, we review the histogram thresholding based image segmentation techniques, namely, Otsu's method and maximum entropy-based segmentation, for target detection in TWRI.

Consider an image of size $N \times M$, whose pixels can assume an intensity value from the set {0, 1, ...,L–1}, where L denotes the total number of intensity levels. Consider the histogram of the image as a discrete probability density function (pdf) $\rho(i)$,

$$\rho(i) = \frac{f_i}{NM}; \quad \rho(i) \geq 0; \quad \sum_{i=0}^{L-1} \rho(i) = 1 \tag{1}$$

where f_i is the frequency of intensity level i.

2.1 Otsu's Method

Otsu's method segments an image into two regions by determining a threshold value T_O that maximizes the sum of class variances[9, 13]

$$T_O = \arg\max_d \{ p_{r_1}(d)[m_{r_1}(d) - m_I]^2 + p_{r_2}(d)[m_{r_2}(d) - m_I]^2 \}, \tag{2}$$

where m_I is the mean image intensity, r_1 and r_2 are the two regions of the image histogram relative to the intensity level d, $p_{r_1}(d)$ and $p_{r_2}(d)$ are the respective region probabilities, which are expressed as

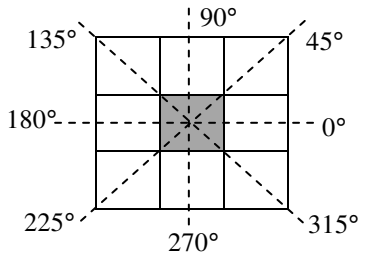

Figure 2. Angular nearest neighbors

$$p_{r_1}(d) = \sum_{i=0}^{d} \rho(i); \quad p_{r_2}(d) = \sum_{i=d+1}^{L-1} \rho(i) \tag{3}$$

and $m_{r_1}(d)$ and $m_{r_2}(d)$ are the means of the respective regions, which are given by

$$m_{r_1}(d) = \sum_{i=0}^{d} \frac{i\rho(i)}{p_{r_1}(d)}; \quad m_{r_2}(d) = \sum_{i=d+1}^{L-1} \frac{i\rho(i)}{p_{r_2}(d)} \tag{4}$$

2.2 Maximum Entropy Based Segmentation

The entropy-based segmentation determines the threshold value T_H by maximizing the sum of class entropies. Based on the information derived from the image histogram, the entropy of the two regions is maximized using the following equation[10, 13]

$$T_H = \arg\max_d \{H_{r_1}(d) + H_{r_2}(d)\}, \tag{5}$$

where $H_{r_1}(d)$ and $H_{r_2}(d)$ are the respective region entropies, which are expressed as

$$H_{r_1}(d) = -\sum_{i=0}^{d} \frac{\rho(i)}{p_{r_1}(d)} \ln \frac{\rho(i)}{p_{r_1}(d)}; \quad H_{r_2}(d) = -\sum_{i=d+1}^{L-1} \frac{\rho(i)}{p_{r_1}(d)} \ln \frac{\rho(i)}{p_{r_1}(d)} \tag{6}$$

with $p_{r_1}(d)$ defined in (3).

3. TEXTURAL FEATURE BASED TARGET DETECTION

The histogram-based methods do no utilize any information regarding the relative spatial position of image pixels. Textural features, on the other hand, contain information about the spatial arrangement of pixel intensities in an image or a selected region of the image. Texture plays an important role in human vision and is one of the important characteristics used in image classification and pattern recognition. A variety of methods have been proposed in the literature for capturing the textural features in an image, such as gray-level co-occurrence matrix, gray-level run length matrix, Fractals, Gabor filters, and the wavelet transform.[11, 14-18] In this paper, we consider the commonly used GLCM features to discriminate between target regions and ghost/clutter regions in through-the-wall radar imagery.

3.1 Gray Level Co-occurrence Matrix (GLCM)

A co-occurrence matrix is defined as a two-dimensional histogram of gray levels for a pair of pixels, which are separated by a fixed spatial relationship. GLCM's are typically computed for various values of distance δ and angle θ between neighboring image pixel pairs. Each pixel, excluding those on the periphery of an image, has eight angular neighboring pixels, as illustrated in Figure 2 for the case of $\delta = 1$. Thus, there are eight possible values for θ, ranging from 0° to 315° in 45° increments. The parameter δ can take positive integer values. However, use of a relatively large δ value may not capture detailed textural information. The general consensus is that highest classification accuracies are obtained for δ = 1 and 2.[19]

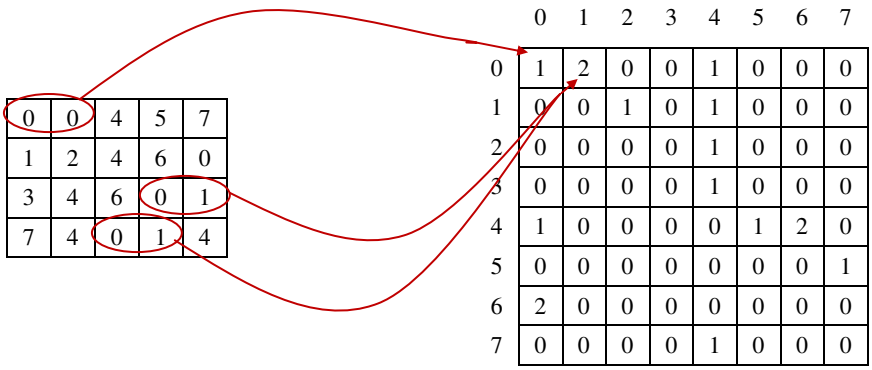

Figure 3. Example of constructing the co-occurrence matrix for $\delta = 1$ and $\theta = 0^\circ$; (a) Image with 8 gray levels, (b) The corresponding 8×8 co-occurrence matrix.

With L as the total number of intensity levels in the image under consideration, the (p, q)-th element of an $L \times L$ GLCM $\mathbf{G}_{\delta,\theta}$, corresponding to specific δ and θ, is the relative frequency with which two θ° neighboring pixels separated by adistance δ occur in the image, one with gray level p, and the other with gray level q. Figure 3 illustrates the process of constructing a GLCM corresponding to $\delta = 1$ and $\theta = 0^\circ$. In Fig. 3(b), element (0, 0) of the co-occurrence matrix takes the value 1 because there is only one instance in the input image of Fig. 3(a), where two 0° adjacent pixels both have the intensity value 0. Likewise, since there are two instances where two 0° adjacent pixels have the values 0 and 1, element (0, 1) of the co-occurrence matrix contains the value 2. The rest of the GLCM elements are populated in a similar fashion.

Based on the definition of GLCM, the co-occurrence matrix for 180° is the transpose of that corresponding to 0° for a given distance δ. The same is true for the angular pairs, 45° and 225°, 90° and 270°, and 135° and 315°. Due to this redundancy, the available choices for the parameter θ reduce to 0°, 45°, 90°, and 135°. As such, the GLCM's for angles 0°, 45°, 90°, and 135° can be formally defined as

$$\mathbf{G}_{\delta,0}(p,q) = \sum_{n=1}^{N}\sum_{m=1}^{M}\begin{cases}1 & \text{if } I(n,m) = p \text{ and } I(n,m+\delta) = q \\ 0 & \text{otherwise}\end{cases} \tag{7}$$

$$\mathbf{G}_{\delta,45}(p,q) = \sum_{n=1}^{N}\sum_{m=1}^{M}\begin{cases}1 & \text{if } I(n,m) = p \text{ and } I(n-\delta,m+\delta) = q \\ 0 & \text{otherwise}\end{cases} \tag{8}$$

$$\mathbf{G}_{\delta,90}(p,q) = \sum_{n=1}^{N}\sum_{m=1}^{M}\begin{cases}1 & \text{if } I(n,m) = p \text{ and } I(n-\delta,m) = q \\ 0 & \text{otherwise}\end{cases} \tag{9}$$

$$\mathbf{G}_{\delta,135}(p,q) = \sum_{n=1}^{N}\sum_{m=1}^{M}\begin{cases}1 & \text{if } I(n,m) = p \text{ and } I(n-\delta,m-\delta) = q \\ 0 & \text{otherwise}\end{cases} \tag{10}$$

where $p, q = 0,1,\ldots,L-1$.

After constructing the GLCM for a given δ and θ, we normalize the GLCM so that the sum of its elements is equal to 1. That is, the (p, q)-th element of the normalized GLCM is given by

$$\overline{\mathbf{G}}_{\delta,\theta}(p,q) = \frac{\mathbf{G}_{\delta,\theta}(p,q)}{\sum_{p=0}^{L-1}\sum_{q=0}^{L-1}\mathbf{G}_{\delta,\theta}(p,q)} \tag{11}$$

Then, $\overline{\mathbf{G}}_{\delta,\theta}(p,q)$ is the joint probability of occurrence of pixel pairs with a defined spatial relationship having gray level values p and q in the image.

3.2 Feature Extraction

Four different features, namely, contrast, correlation, energy and homogeneity, are extracted from each normalized GLCM.[11, 19] *Contrast* measures the amount of local intensity variations present in the image and is defined as

$$Contrast = \sum_{p,q} | p-q |^2 \, \overline{\mathbf{G}}_{\delta,\theta}(p,q) \tag{12}$$

The c*orrelation* feature is a measure of gray level linear dependencies in the image and is given by

$$Correlation = \sum_{p,q} \frac{(p-\mu_x)(q-\mu_y)\overline{\mathbf{G}}_{\delta,\theta}(p,q)}{\sigma_x \sigma_y} \tag{13}$$

where μ_x, σ_x, and μ_y, σ_y are the means and standard deviations of the respective marginal distributions $\overline{\mathbf{G}}^{x}_{\delta,\theta}(p) = \sum_{q} \overline{\mathbf{G}}_{\delta,\theta}(p,q)$ and $\overline{\mathbf{G}}^{y}_{\delta,\theta}(q) = \sum_{p} \overline{\mathbf{G}}_{\delta,\theta}(p,q)$ associated with the normalized GLCM. The *energy* feature measures the textural uniformity and is defined as

$$Energy = \sum_{p,q} (\overline{\mathbf{G}}_{\delta,\theta}(p,q))^2 \tag{14}$$

Finally, the *homogeneity* feature measures the closeness of the distribution of elements in the co-occurrence matrix to the co-occurrence matrix diagonal. It is defined as

$$Homogeneit\,y = \sum_{p,q} \frac{1}{1+|p-q|} \overline{\mathbf{G}}_{\delta,\theta}(p,q) \tag{15}$$

For the behind-the-wall target detection problem, the aforementioned textural features are extracted from the 0°, 45°, 90°, and 135° nearest-neighbor ($\delta = 1$) GLCM's. Therefore, the length of the resulting feature vector is 16. It is noted that, instead of the entire image, the textural feature vectors are computed only for those regions of the image which are identified as candidate target regions after the image segmentation step.

3.3 Mahalanobis Distance Metric

Let Ω_T, Ω_C be the target and clutter classes with respective means and covariance matrices denoted by $\boldsymbol{\mu}_T$, $\mathbf{C}_T$, and $\boldsymbol{\mu}_C$, $\mathbf{C}_C$, and defined as

$$\begin{aligned} \boldsymbol{\mu}_T &= E(\mathbf{x}_T),\ \mathbf{C}_T = E((\mathbf{x}_T - \boldsymbol{\mu}_T)(\mathbf{x}_T - \boldsymbol{\mu}_T)^T],\ \ \mathbf{x}_T \in \Omega_T \\ \boldsymbol{\mu}_C &= E(\mathbf{x}_C),\ \mathbf{C}_C = E((\mathbf{x}_C - \boldsymbol{\mu}_C)(\mathbf{x}_C - \boldsymbol{\mu}_C)^T],\ \ \mathbf{x}_C \in \Omega_C \end{aligned} \tag{16}$$

With $\mathbf{x}$ representing a feature vector extracted from a candidate target image region, the Mahalanobis distance R_T of $\mathbf{x}$ to the target class is defined as,[20]

$$R_T^2 = (\mathbf{x}-\boldsymbol{\mu}_T)^T \mathbf{C}_T^{-1} (\mathbf{x}-\boldsymbol{\mu}_T) \tag{17}$$

while the Mahalanobis distance R_C of $\mathbf{x}$ to the clutter class is given by

$$R_C^2 = (\mathbf{x}-\boldsymbol{\mu}_C)^T \mathbf{C}_C^{-1} (\mathbf{x}-\boldsymbol{\mu}_C) \tag{18}$$

The following decision rule is applied to classify the feature vector $\mathbf{x}$,

$$\mathbf{x} \in \begin{cases} \Omega_T & \text{if } R_T^2 < R_C^2 \\ \Omega_C & \text{otherwise} \end{cases} \tag{19}$$

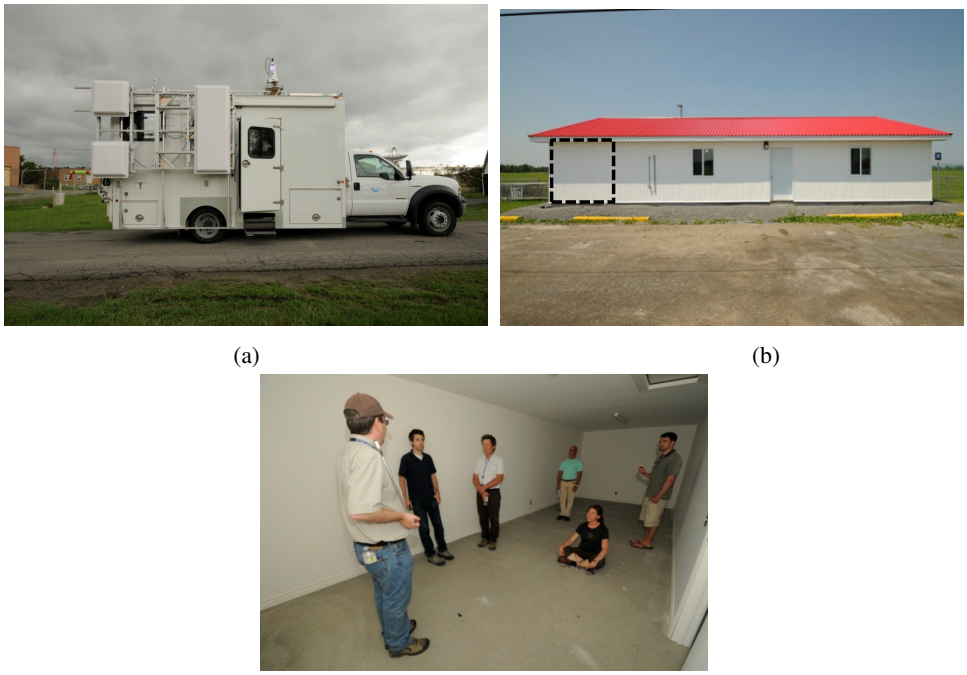

(a) (b)

(c)

Figure 4. (a) Through-the-wall MIMO System. (b) Building used for Through-the-Wall Measurements (the dashed square indicates the room containing the human targets. (c) Scene layout. Photos by J. Lang, DRDC Ottawa.

4. EXPERIMENTAL RESULTS

We evaluate both the image segmentation only and the feature based methods using real 2D images collected with the 3D experimental through-the-wall multiple-input multiple output (MIMO) radar testbed developed by DRDC. The radar is installed inside a vehicle with its two transmit antennas and an eight-element receive array mounted on the side of the vehicle, as shown in Fig. 4(a). The antenna elements are compact Y-shaped printed bowtie antennas[21] and, when used in the vertical polarization, have approximately 60º beamwidth in elevation and 150º beamwidth in azimuth. The receive array has an inter-element spacing of 15 cm, and the two transmit antennas are separated by 1.2 m. The transmit and receive array antennas have a horizontal spacing of 2 m. A frequency-modulated continuous wave (FMCW) signal covering the 0.8 to 2.7 GHz frequency band is used as the transmit signal.[12] A switch is used to alternate the radar transmissions between the two transmit antennas, and the eight-channel radar receiver digitizes the eight received signals for each radar transmission. The scene being imaged consisted of a small room in the Troop Shelter building with six human occupants (see Fig. 4(b)). One of the targets was sitting on the floor while the others were all standing at various locations inside the room, as shown in Fig. 4(c). The exterior walls of the building were constructed of vinyl, chip board and drywall on a 16in. spacing wood stud frame. The raw radar data were collected while the vehicle moved along a straight path parallel to the front wall of the building, allowing 3D images to be generated in downrange, azimuth, and elevation.

A collection of multiple parallel 2D images constituting vertical slices (azimuth vs. elevation) of the 3D scene was used for performance evaluation of the proposed scheme. Figure 5 shows the azimuth vs. elevation images corresponding to the downrange locations of each of the six targets. We observe from Fig. 5 that the targets are clearly visible in some of the images, whereas in other images, the targets are accompanied by strong clutter and multipath ghosts, which are quite similar to the imaged targets. Figure 6 shows the corresponding binary images obtained after application of the maximum entropy based image segmentation. As expected, the image segmentation scheme failed to recover only the targets and mistakenly captured multipath ghosts and clutter that appeared similar to the targets. Otsu's method (not shown) provided similar results.

The binary images in Fig. 6 were then used as masks on the original images to produce the resulting enhanced images, identifying candidate target regions. Next, the candidate target regions were extracted, which constituted the testing

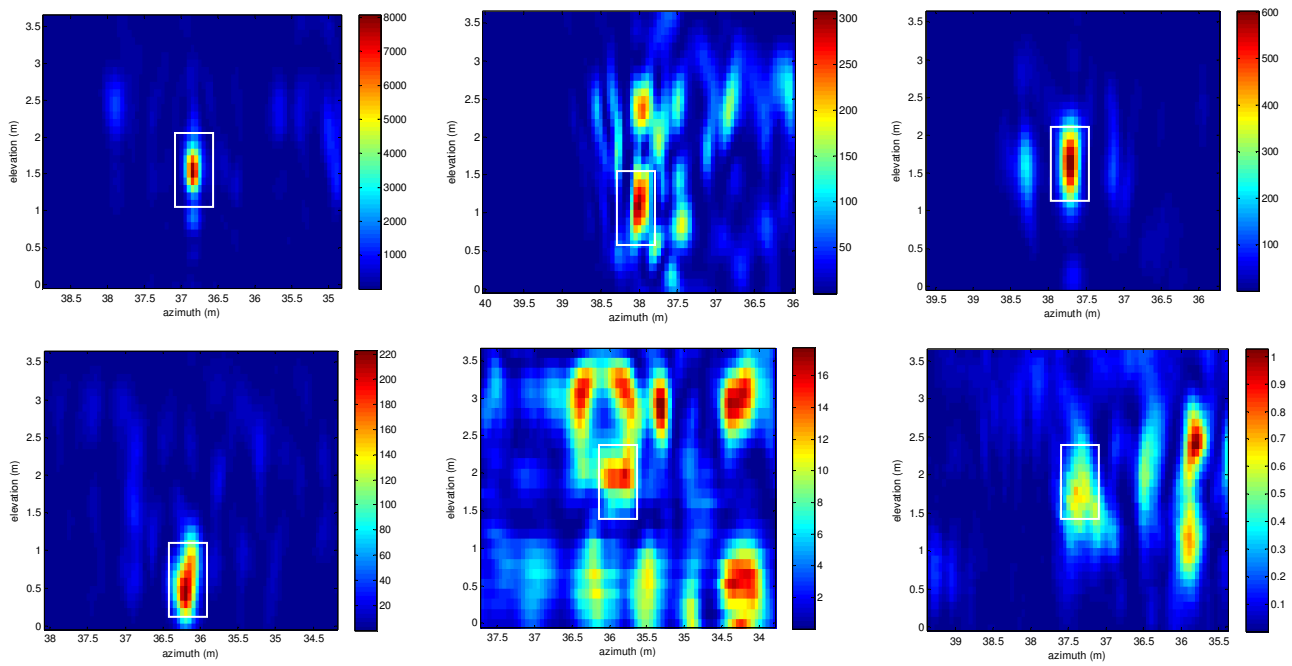

Figure 5. Azimuth vs. Elevation images corresponding to the downrange locations of six human targets. The true target in each image is indicated by a white rectangle.

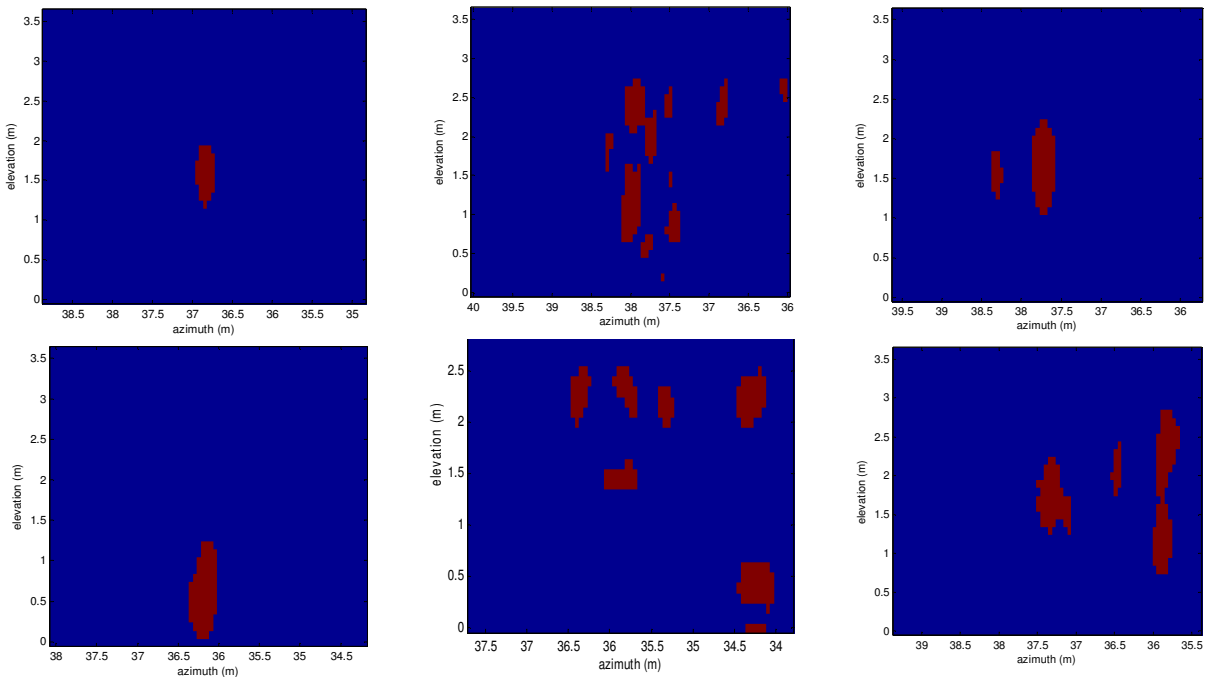

Figure 6. Binary images (azimuth vs. elevation) corresponding to the downrange locations of the six human targets after application of entropy based segmentation method.

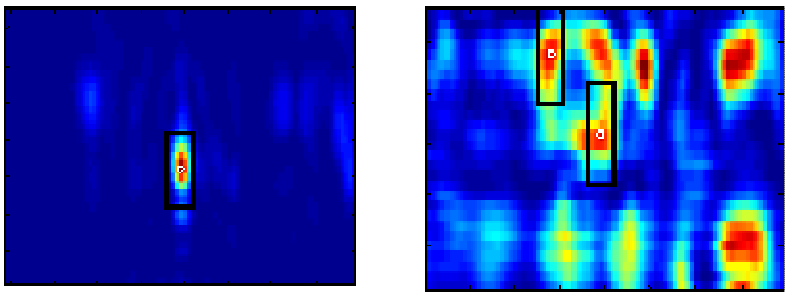

Figure 7. Feature based Target Detection Results for the test images (Top left and bottom center images of Fig. 5). Each region identified as a target is indicated by a black rectangle on the original azimuth vs. elevation images corresponding to the downrange locations of the human targets.

dataset, and the 16-element textural feature vectors were computed for each of the candidate targets. The training dataset consisted of i) 4 target and 4 clutter regions chosen from the testing dataset, and ii) additional 16 target and 16 clutter regions selected from the neighboring vertical images. The Mahalanobis distance of the target candidate feature vectors to the target and clutter classes was computed and the candidates were classified in accordance with the minimum distance decision rule. Figure 7 depicts the feature based detector results by indicating the regions classified as targets with a black rectangle only for those original images which were not part of the training dataset. We observe that the feature based detector has been successful in detecting both targets while causing only one false alarm. As expected, the candidate regions that were part of the training dataset were also correctly classified. Use of a larger number of independent vertical images was not possible for this limited study, but will be required in further investigations.

5. CONCLUSION

In this paper, we presented a textural feature based target detection scheme for detecting stationary human targets in through-the-wall radar imagery. Histogram thresholding based image segmentation was first applied to the images in order to reduce the background noise and clutter regions. Several textural features, such as contrast, correlation, energy, and homogeneity, were then extracted from the 0°, 45°, 90°, and 135° nearest-neighbor GLCM's of the candidate target regions identified by the image segmentation step. A minimum distance classifier based on the Mahalanobis distance metric was employed to distinguish between the targets and multipath ghosts and clutter that mimicked the targets in intensity and shape. The performance of the proposed scheme was evaluated using real 2D images. The results showed that the image segmentation step was able to remove only those clutter regions that were distinct from the target regions, while the proposed follow-on step of textural feature based classification provided an enhanced performance by maintaining high target and low clutter/ghost levels in the segmented images. Further work calls for the collection of a training dataset consisting of a larger number of independent images, comparison with the neural network based classifiers, and testing with data collected through a variety of walls for investigating robustness issues.

ACKNOWLEDGMENT

This work was supported by DRDC under Contract W7714-125544/00 l/SV.

REFERENCES

[1] Amin, M., [Through the Wall Radar Imaging], CRC Press, Boca Raton, (2010).
[2] Amin, M. G. and Ahmad, F., "Wideband synthetic aperture beamforming for through-the-wall imaging," IEEE Signal Process. Mag. 25(4), 110–113 (2008).
[3] Setlur, P., Amin, M. and Ahmad, F., "Indoor Imaging of targets enduring simple harmonic motion using Doppler radars," Proc. Int. Symp. Signal Process. Information Tech., Athens, Greece, December 2005.
[4] Setlur, P., Ahmad, F. and Amin, M., "Analysis of micro-Doppler signals using linear FM basis decomposition," Proc. SPIE, Orlando, FL, April 2006.

[5] Amin, M. G., Setlur, P., Ahmad, F., Sevigny, P. and DiFilippo, D., “Histogram based segmentation for stationary indoor target detection,” Proc. SPIE, Baltimore, MD, April 2012.
[6] Seng, C. H., Amin, M. G., Ahmad, F. and Bouzerdoum, A., "Segmentations of through-the-wall radar images," Proc. IEEE Radar Conf., (2012).
[7] Seng, C. H., Amin, M. G., Ahmad, F. and Bouzerdoum, A., "Image segmentations for through-the-wall radar target detection," IEEE Trans. Aerosp. Electronic Syst. 49(3), (2013).
[8] Mostafa, A.A and Zoubir, A.M., “3D target detection in through-the-wall radar imaging,” Proc. SPIE 7697, p. 76971F.
[9] Otsu, N., "A threshold selection method from gray-level histogram," IEEE Trans. Systems, Man and Cybernetics 9(1), 62-66 (1979).
[10] Kapur, J., Sahoo, P. and Wong, A., "A new method for gray-level picture thresholding using the entropy of the histogram," Computer Vision, Graphics, and Image Process. 29(3), 273-285 (1985).
[11] Harlick, R. M., Shanmugam, K. and Dinstein, I.,“Textural features for image classification,” IEEE Trans. Systems, Man, Cybernetics SMC-3(6), 610-621 (1973).
[12] Sévigny, P., DiFilippo, D., Laneve, T., Chan, B., Fournier, J., Roy, S., Ricard, B. and Maheux, J., "Concept of operation and preliminary experimental results of the DRDC through-wall SAR system," Proc. SPIE 7669, 766907-1-766907-11 (2010).
[13] Sezgin, M. and Sankur, B., “Survey over image thresholding techniques and quantitative performance evaluation,” J. Electronic Imaging 13(1), 146–165, 2004.
[14] Reed, T.R. and Dubuf, J.M.H., “A review of recent texture segmentation and feature extraction techniques,” CVGIP: Image Understanding 57(3), 359-372 (1993).
[15] An-Zen Shih, Sie Jheng-Huei and Peng Kaiyang, “Image classification by using a hybrid fractal-based method,” Proc. Int. Conf. on Machine Learning and Cybernetics 4, 1800-1803 (2011).
[16] Idrissa M. and Acheroy M, “Texture classification using Gabor filters,” Pattern Recognition Letters 23(7), 1095-1102 (2002).
[17] Ciesielski, V., Lam, B. and Minh Luan Nguyen, “Comparison of evolutionary and conventional feature extraction methods for malt classification,” Proc. IEEE Congress Evolutionary Computation, 1-7 (2012).
[18] Lukashevich, M. and Sadykhov, R., “Texture analysis: Algorithm for texture features computation,” Proc. Intl. Conf. Problems of Cybernetics and Informatics, 1-3 (2012).
[19] Gadkari, D., [Image quality analysis using GLCM], M.S. Thesis, University of Central Florida, Orlando, FL, 2004.
[20] Duda, R. O. and Hart, P. E., [Pattern Classification], Wiley, 2nd Ed., 2000.
[21] Raut, S. and Petosa, A., "A compact printed bowtie antenna for ultra-wideband applications," Proc. European Microwave Conf., 81-84 (2009).